Neurocomputing 151 (2015) 161–167

Contents lists available at ScienceDirect

Neurocomputing

journal homepage: www.elsevier.com/locate/neucom

Fully automatic segmentation of ultrasound common carotid artery images based on machine learning

Rosa-María Menchón-Lara *, José-Luis Sancho-Gómez

Dpto. Tecnologías de la Información y las Comunicaciones, Universidad Politécnica de Cartagena, Plaza del Hospital, 1, 30202 Cartagena, Murcia, Spain

ARTICLE INFO

Article history:
Received 12 May 2014
Accepted 23 September 2014
Available online 18 October 2014

Keywords:
Pattern recognition
Auto-encoders
Deep learning
Atherosclerosis
Ultrasound imaging
Intima-media thickness

ABSTRACT

Atherosclerosis is responsible for a large proportion of cardiovascular diseases (CVD), which are the leading cause of death in the world. The atherosclerotic process is a complex degenerative condition mainly affecting the medium- and large-size arteries, which begins in childhood and may remain unnoticed during decades. It causes thickening and the reduction of elasticity in the blood vessels. An early diagnosis of this condition is crucial to prevent patients from suffering more serious pathologies (heart attacks and strokes). The evaluation of the Intima-Media Thickness (IMT) of the Common Carotid Artery (CCA) in B-mode ultrasound images is considered the most useful tool for the investigation of preclinical atherosclerosis. Usually, it is manually measured by the radiologists. This paper proposes a fully automatic segmentation technique based on Machine Learning and Statistical Pattern Recognition to measure IMT from ultrasound CCA images. The pixels are classified by means of artificial neural networks to identify the IMT boundaries. Moreover, the concepts of Auto-Encoders (AE) and Deep Learning have been included in the classification strategy. The suggested approach is tested on a set of 55 longitudinal ultrasound images of the CCA by comparing the automatic segmentation with four manual tracings.

1. Introduction

Cardiovascular diseases (CVD) represent the major cause of death and disability worldwide. Atherosclerosis is responsible for a large proportion of CVD [1]. It is a chronic degenerative disease characterized by the accumulation of fatty material and cholesterol at the arterial walls. Therefore, atherosclerosis causes thickening and the reduction of elasticity in the arterial walls. Although this pathology may remain unnoticed for decades, atherosclerotic lesions (plaques) could even lead to a total occlusion of the blood vessels. This is the major underlying cause of heart attacks and strokes. For this reason, an early diagnosis and follow up of the atherosclerosis is crucial for preventive purposes. In this sense, the Intima-Media Thickness (IMT) of the Common Carotid Artery (CCA) is considered as an early and reliable indicator of this condition [2].

The IMT is measured by means of a B-mode ultrasound scan, which is a noninvasive , relatively inexpensive, and widely available technique that allows a short time examination. However, resolution and contrast of ultrasound images are generally poor. These images are affected by the multiplicative speckle noise, which tends to reduce the image quality, obscuring and blurring diagnostically important details. The use of different protocols and the variability between observers are recurrent problems in the IMT measurement procedure. Repeatability and reproducibility of the process are of great significance to study the IMT [3,4]. For these reasons, IMT should be measured preferably on the far wall of the CCA within a region free of plaque [2]. The optimal measurement section (1 cm long) is located at least 5 mm below the carotid bifurcation, where a double-line pattern corresponding to the intima-media-adventitia layers can be clearly observed. As can be seen in Fig. 1, the IMT is the distance between the lumen-intima (LI) interface and the media-adventitia (MA) interface.

Usually, delineations of the CCA are manually performed by medical experts. By means of image segmentation algorithms it is possible to reduce the subjectivity and variability of manual approaches and detect the IMT throughout the artery length. In the last two decades, several solutions have been developed to perform the carotid wall segmentation in ultrasound images [5]. Most of the proposed methods are not completely automatic and they require user interaction to start the algorithm, such as [6–10]. However, some fully automatic approaches were recently published [11–15]. It is possible to make a classification of techniques according to the used methodology. In this sense, we can find algorithms based on edge detection and gradient-based techniques [6,8,9,16], and other proposals based on dynamic programming [17–22], active contours [7,12,23–28], neural networks [11] or in a

* Corresponding author.
E-mail address: rmml@alu.upct.es (R.-M. Menchón-Lara).

http://dx.doi.org/10.1016/j.neucom.2014.09.066
0925-2312/

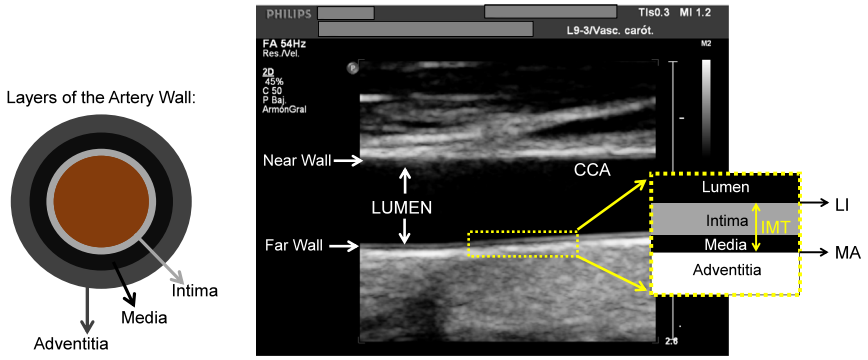

Fig. 1. Diagram of the artery wall (left) and longitudinal view of the CCA in a B-mode ultrasound image (right).

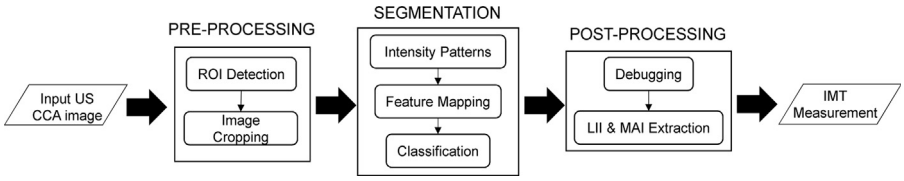

Fig. 2. Overview of the proposed method for carotid wall segmentation and IMT measurement.

combination of techniques [10,29,14]. There are also highlight techniques based in statistical modeling [30,31] or in Hough transform [13,32].

In this work, a fully automatic segmentation technique based on Machine Learning and Statistical Pattern Recognition is proposed to measure IMT from ultrasound CCA images. Firstly, a given image is pre-processed to detect the region of interest (ROI). Then, pixels belonging to the ROI are classified by means of artificial neural networks to identify the LI and MA interfaces. The concepts of Auto-Encoders (AE) and Deep Learning have been included in this classification stage. Finally, the obtained results are post-processed to extract the final contours for the IMT measurement. The automatic measures of the IMT have been compared with the values obtained from different manual segmentations and the statistical analysis of this comparison shows the accuracy of the proposed method.

The remainder of this paper is structured as follows: Section 2.1 describes the dataset of ultrasound CCA images and the manual segmentations. In Section 2.2, the proposed segmentation method is explained in detail. The obtained results are shown in Section 3. Finally, the main extracted conclusions close the paper.

2. Materials and methods

2.1. Ultrasound image acquisition and manual segmentations

A set of 55 longitudinal B-mode ultrasound images of the CCA have been used in this work. All of them were provided by the Radiology Department of *Hospital Universitario Virgen de la Arrixaca* (Murcia, Spain). Fig. 1 (right) shows an example of the tested ultrasound images. Ultrasound scans were acquired using a *Philips iU22 Ultrasound System* by means of three different ultrasound transducers (*L*12-5, *L*9-3 and *L*17-5) and recorded digitally with 256 gray levels. The spatial resolution of the images ranges from 0.033 to 0.066 mm/pixel, with mean and standard deviation equal to 0.051 and 0.015 mm/pixel, respectively. The parameters of the scanner were adjusted in each case by the radiologist. Some blurred and noisy images, affected by intraluminal artifacts, and some others with partially visible boundaries are included in the studied set.

To assess the performance of the proposed segmentation method and the accuracy of the obtained IMT measurements, it is necessary to compare the automatic results with some indication of reference values (*ground-truth*, GT). In this case, the GT corresponds with the average of four different manual segmentations for each ultrasound image. In particular, two experienced radiologists delineated the 55 images twice, with a mean period of two months between tracings. Each manual segmentation of a given ultrasound image includes tracings for the LI and MA interfaces on the far carotid wall.

2.2. Carotid ultrasounds segmentation

Fig. 2 shows an overview of the proposed IMT segmentation methodology. Firstly, a given ultrasound CCA image is pre-processed to automatically detect the region of interest (ROI), which is the far wall of the blood vessel. As result of this stage, a cropping of the input ultrasound image is obtained (ROI image). Then, a windowing process takes place on the ROI image in order to construct the intensity pattern corresponding to each pixel (intensity values from a neighbourhood). After this, different auto-encoders provide compressed representations of these intensity patterns in a lower dimensional feature space. The new features are classified by means of artificial neural networks to separately detect the LI and MA interfaces. Finally, classification results are post-processed to extract the final contours on which the IMT is measured.

2.2.1. Pre-processing of ultrasound CCA images

In the carotid ultrasound images (see Fig. 1), the lumen corresponds to a dark region (low echogenicity) delimited by the arterial walls. Over the lumen in the picture, at less depth, it is observed the echo corresponding to the near wall. The far wall, where the IMT is measured, is located below the lumen, and it constitutes the region of interest (ROI).

The aim of the pre-processing stage is the location of the carotid far wall in a completely automatic way. In particular, a binary mask is built using morphological operations [33] to locate the carotid lumen. Once the lumen has been located, we focus on its lower limit corresponding to the far wall of the CCA and the

boundaries of the ROI are established. The superior boundary is fixed to 0.6 mm above the upper point of the far wall detected in the binary mask, whereas the bottom boundary is fixed to 1.5 mm below the lower point. As result of this stage, a cropping of the input ultrasound image is obtained (ROI image). For more details about this stage consult [11].

2.2.2. Segmentation by means of pattern recognition with neural networks

Segmentation is one of the most difficult tasks in nontrivial image processing. Since segmentation can be considered as a classification of pixels, it is often treated as a pattern recognition problem and addressed with related techniques [34]. This section describes the main stage of the proposed method, in which artificial Neural Networks (NN) carry out the segmentation of the ultrasound CCA images. The NN used in this work are standard *Multi-Layer Perceptrons* (MLP), with a single hidden layer, trained under the *Scaled Conjugate Gradient* (SCG) learning rule [35].

The initial idea consists of training NN to classify the pixels from the ultrasound images by considering the intensity values of a neighbourhood of the pixel to classify [11]. The neighbourhoods considered in this study are vertically oriented rectangular windows (13×3 pixels), since the '*bright-dark-bright*' intensity pattern corresponding to the IMT can be found in the vertical direction of the images. The reason for choosing a window height of 13 pixels is that for the used set of 55 ultrasound CCA images, the mean IMT is about 13 pixels. Therefore, this neighbourhood will provide the best contextual information about the pixel to be classified. After the appropriate learning process, a given network will be able to recognize the pixels belonging to the IMT boundaries (i.e., LI and MA interfaces). Furthermore, in this paper, the concepts of Auto-Encoders (AE) and Deep Learning have been incorporated to the original scheme. Fig. 3 shows the proposed configuration. As can be seen in the scheme, the processing of each IMT boundary (LI and MA interfaces) is separately performed.

Auto-Encoders 1 and 2 are artificial NN used for learning efficient codifications. AE learns to represent features in a dataset meaningfully, typically for the purpose of dimensionality reduction [36]. It was shown that those are more efficient that other methodologies such as Principal Component Analysis (PCA) [37]. The AE proposed here are MLP performing unsupervised learning, in which input data is used as output data (see Fig. 4). Then, in the hidden layer of the AE take place a feature mapping. In our particular case, $M < d$ (number of hidden neurons < input data dimension, see Fig. 4), and a compressed representation of the data is obtained at the output of the AE hidden layer. These outputs of the hidden layer are then used as input data to another MLP (NN_1 or NN_2 in Fig. 3) for its classification.

A dataset is needed to perform the training of the different NN. To ensure a good generalization capability of the networks, five heterogeneous images were carefully chosen (with different orientations of the CCA, spatial resolutions, IMT measures, etc.) to assemble a representative and consistent dataset. It is necessary to emphasize that using all the pixels/patterns in a selected image for training is inappropriate, since the dataset would be extremely large and highly imbalanced. In our case, the dataset was assembled by taking samples from the five manually segmented images selected for this purpose. Finally, it consists of 12,900 patterns: 3100 of them (24%) are from class '*LII-pixels*'; 3350 (26%) are from class '*MAI-pixels*'; and the remaining (50%) are from class '*non-IMT-boundary*'. During the learning process, the dataset was randomly divided into three subsets: 50% of samples for training, 20% for validation (stopping criterion and network size selection) and 30% for testing.

As commented above, the LI and MA interfaces are separately detected. For the LI interface, AE_1 is trained to obtain compressed representations of the patterns corresponding to pixels belonging to the LI interface (3100 patterns with a dimension of $13 \times 3 = 39$ features). The learning process is repeated varying the number of hidden neurons of the AE_1 from 2 to 39. Then, the whole dataset (12,900 patterns) is passed through the AE_1 and the hidden layer outputs are used to train NN_1, which performs a binary classification between '*LII-pixels*' and '*non-LII-pixels*'. On the other hand, AE_2 performs a feature mapping for patterns corresponding to pixels belonging to the MA interface (3350 patterns with 39 features). Once its training is carried out, the 12,900 samples are processed with AE_2. The transformed features (hidden layer outputs) are used in the learning process of the NN_2, which performs another binary classification between '*MAI-pixels*' and '*non-MAI-pixels*'.

Moreover, as it shown in Fig. 3, two neighbourhoods have been considered. For both AE_1 and AE_2, the input patterns consist of 39 features (13×3 window). However, whereas for AE_2 the neighbourhood is centred on the pixel to be classified, for the AE_1 the neighbourhood is vertically displaced until the pixel to classify is located at the central position of the window base. This is done with the purpose of providing a better characterization of the '*LII-pixels*' to AE_1 (large dark area corresponding to the lumen above the pixel).

As shown in Section 3.1, the use of auto-encoders allows a significant reduction in the dimension of the features space (from 39 to 11 for AE_1, and from 39 to 9 for AE_2). Fig. 7 (central) shows the final classification results for an ultrasound CCA image, according to the proposed classification scheme. As can be seen, the LI and MA interfaces are correctly identified in the image. Nevertheless, it is still necessary to eliminate some residues and to refine the contours in order to assess the IMT. To this end, a post-processing stage has been designed (detailed in Section 2.2.3).

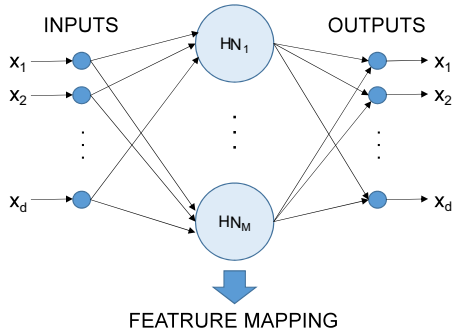

Fig. 4. Structure of a generic auto-encoder.

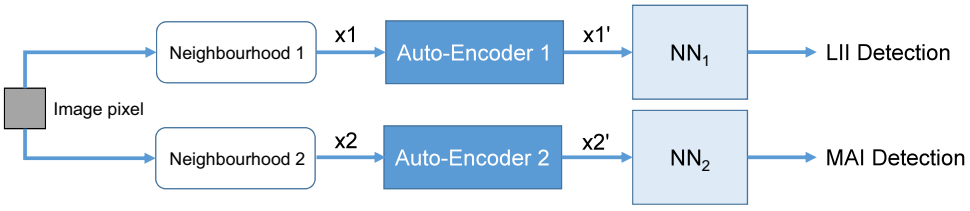

Fig. 3. Strategy adopted to solve the segmentation task.

2.2.3. Post-processing of classification results

The results of the classification stage should be debugged to extract the final LI and MA boundaries, see central image in Fig. 7. It is necessary to identify and discard, as far as possible, the misclassified pixels. In this sense, the relative position between pixels classified as '*LII-pixels*' and those classified as '*MAI-pixels*' provides useful information. Moreover, due to the poor resolution of the ultrasound images, thick boundaries are obtained instead of one-pixel contours. This happens because the networks find the searched intensity patterns in all these pixels. In order to solve this drawback, a simple non-linear data-fitting problem is formulated to find the best polynomial approximation for LI and MA interfaces. This is done by minimizing the squared error between the LII-pixels (or MAI-pixels) in the image and the approximated contour. The bottom image in Fig. 7 shows an example of the final boundaries extracted from the classification results (central image).

3. Results

The suggested segmentation methodology was developed and tested in a PC with a core i7-3770 3.4 GHz processor and 12 GB RAM running MATLAB 2013a. The mean total time per processed image is 1.4 s. The ROI selection task (pre-processing stage) shows high computational efficiency by spending 0.37 s in mean for each case. Once the networks have been trained, classification results are provided in a fast way, with an average response time of 0.48 s for all the pixel in the selected ROI. On the other hand, the post-processing returns the final IMT boundaries in 0.6 s.

3.1. Feature mapping and classification performance

As commented in Section 2.2.2, AE_1 and AE_2 are trained to obtain a compressed representation ($M < d$, see Fig. 4) of the intensity pattern corresponding to each pixel of a given ultrasound CCA image. In each case, the learning process is repeated varying the number of hidden neurons from 2 to 39. For each network size (number of hidden nodes), the corresponding NN_1 and NN_2 (with different dimension of input data) were trained and its performance has been analysed. All designed networks in this study were retrained 30 times with different initial random values of the connection weights. Moreover, the number of hidden neurons in NN_1 and NN_2 is varied from 5 to 100 and the optimal size of each network is selected according to the minimum mean error reached on a validation dataset.

Fig. 5 shows the performance of NN_1 in each case (from 2 to 39 input features). The mean classification accuracy achieved is depicted in the left graph, whereas the mean specificity and sensitivity are shown in the right graphic. NN_1 together with AE_1 outperform the classification accuracy of a MLP trained with the 39-dimensional data (13×3 neighbourhood) to recognize the LI interface (dashed line in Fig. 5) when considering a feature mapping to 3 or more dimensions. Since the specificity remains constant, the optimal configuration has been chosen by analysing the sensitivity. Thus, the best performance is obtained with 11 input features, i.e. when AE_1 reduces the dimensionality of data from 39 to 11. In a similar way, Fig. 6 shows the performance of NN_2, which was trained to identify '*MAI-pixels*'. In this case, AE_2 and NN_2 achieve a classification accuracy similar to the obtained when considering a 39-dimensional feature space (dashed line). The optimal configuration (best sensitivity) is obtained for 9 input features (feature mapping from 39 to 9 dimensions).

3.2. Segmentation accuracy and IMT measurements

The proposed segmentation method has been tested on a set of 55 B-mode ultrasound images. Some examples of segmented images are shown in Figs. 7 and 8. The final boundaries corresponding to the LI and MA interfaces detected by our automatic segmentation method are superimposed on the ultrasounds. As can be seen, our fully automatic segmentation approach is robust against the orientation and appearance of the CCA in the ultrasound image (slope and curvature).

Given an ultrasound image and two different segmentations (S_1 and S_2) to compare, the degree of agreement between its IMT measures is assessed by calculating the absolute error value:

$$\epsilon^{IMT_i} = |IMT_i^{S_1} - IMT_i^{S_2}| \quad (1)$$

being ϵ^{IMT_i} the IMT measurement error between the segmentation S_1 and the segmentation S_2 for the *i-th* image. In each case, the IMT value, i.e. the distance between the boundaries corresponding to LI and MA, is evaluated by using the Mean Absolute Distance (MAD) metric. The mean and standard deviation values (55 processed images) for the intra-observer ($E1_1$–$E1_2$ and $E2_1$–$E2_2$), inter-observer (E1–E2) and inter-method (A-GT) IMT measurement errors can be seen in Table 1. The mean absolute error of the automatic measurements is about 50 μm, which is a value slightly higher than the intra- and inter-observer errors but it is similar to the obtained by other published methods (see Table 2).

Moreover, Fig. 9 shows the linear regression analysis for the IMT measures between manual and automatic segmentations (right graph), and the Bland–Altman plot of the differences between the IMT of the corresponding two segmentations (manual and automatic) against their average (left graph). The regression analysis

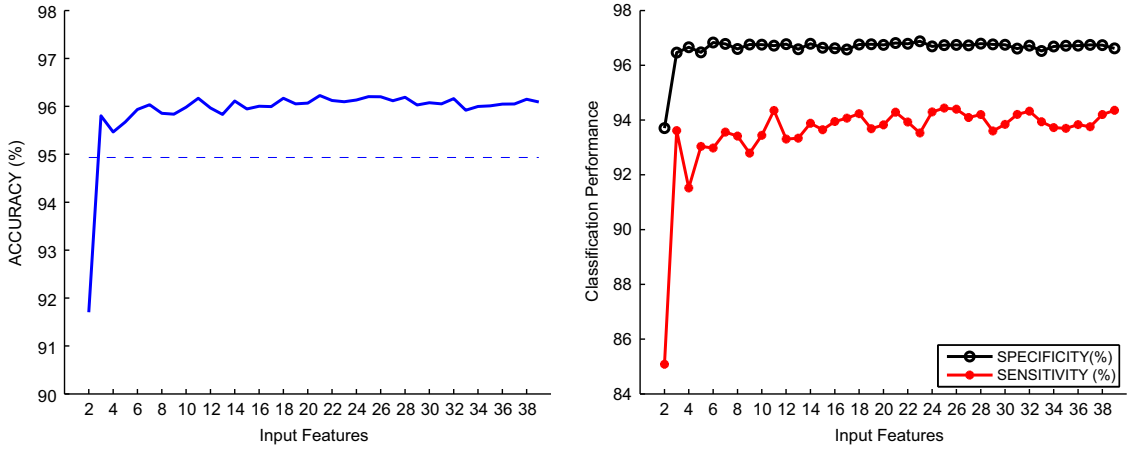

Fig. 5. Performance of NN_1 (trained to detect LII-pixels) for different dimensions of input data: mean classification accuracy (left) and specificity and sensitivity (right).

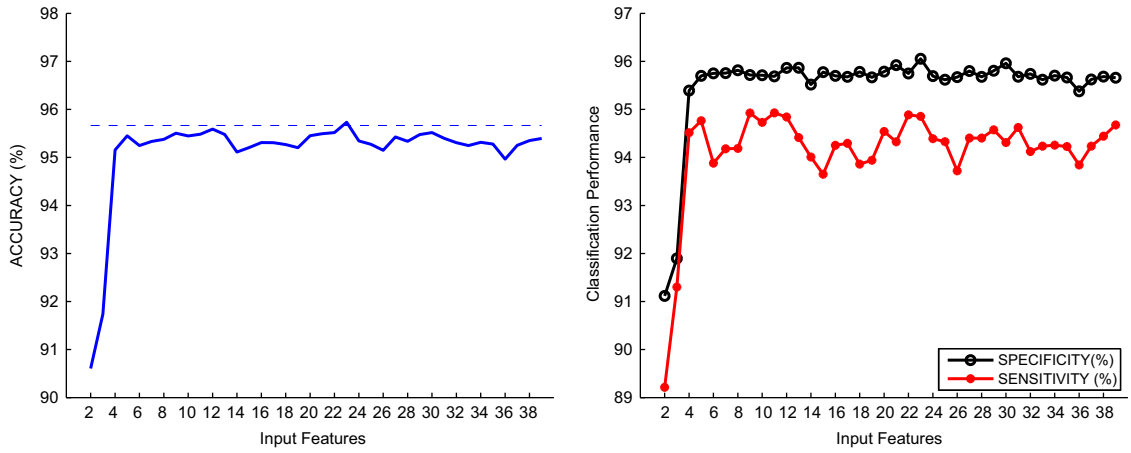

Fig. 6. Performance of NN_2 (trained to detect MAI-pixels) for different dimensions of input data: mean classification accuracy (left) and specificity and sensitivity (right).

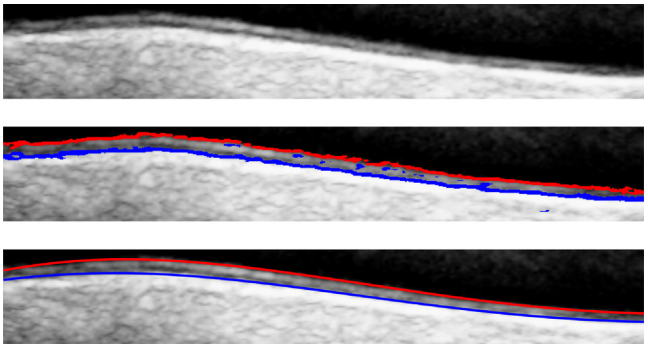

Fig. 7. Example of the results obtained at each stage of the proposed segmentation method: selected ROI in the pre-processing stage (top), classification results (central) and final LI and MA boundaries after the post-processing stage.

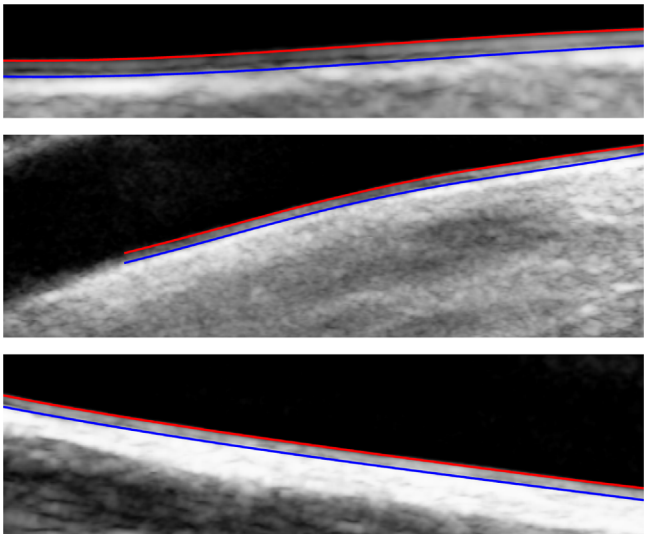

Fig. 8. Different examples of good segmentation. The proposed method is robust against the orientation and appearance of the CCA in the ultrasound image.

shows a high degree of agreement between manual and automatic measurements, with a 93.3 % correlation coefficient. Bland–Altman plot shows the following limits of agreement (mean $\pm 2 \times$ standard deviation): -0.018 ± 0.137 mm. Therefore, the proposed method tends to slightly underestimate the IMT.

Table 1
IMT measurement errors (mm) between different segmentations.

	IMT measurement error	
Compared segmentations	Mean	Std. Dev.
$E1_1$–$E1_2$	0.025	0.018
$E2_1$–$E2_2$	0.027	0.021
E1–E2	0.037	0.069
A-GT	0.050	0.050

Table 2
Comparison with other techniques for the IMT measurement. The metric adopted to assess the IMT and the errors is MAD. *N* is the number of images and the third column shows the spatial resolution of the images in mm/pixel. FA: fully automatic.

Author	*N*	IMT_{GT} (mm)	IMT_{Method} (mm)	ϵ^{IMT} (μm)	FA
Liang [18]	50	0.88 ± 0.25	0.93 ± 0.25	42 ± 25	No
Liguori [6]	20	0.92 ± 0.19	0.92 ± 0.20	15.6 ± 4.2	No
Gutierrez [24]	30	0.63 ± 0.12	0.72 ± 0.14	90 ± 60	No
Stein [8]	50	–	0.67 ± 0.12	40 ± 7	No
Faita [9]	150	0.56 ± 0.14	0.57 ± 0.14	10 ± 35	No
Molinari [14]	182	0.92 ± 0.30	0.75 ± 0.39	54 ± 35	Yes
Xu [32]	50	0.63 ± 0.14	0.65 ± 0.16	38.1 ± 16.4	No
Petroudi [28]	100	0.67 ± 0.14	0.61 ± 0.15	95.0 ± 61.5	No
Menchón-Lara [11]	60	0.64 ± 0.19	0.61 ± 0.19	37.6 ± 25.2	Yes
Proposed method	55	0.62 ± 0.19	0.60 ± 0.19	49.9 ± 49.8	Yes

4. Conclusions

This paper proposes a fully automatic segmentation method of the CCA far wall based on Machine Learning in order to measure the IMT. Segmentation is treated as a pattern recognition problem. Thus, the main stage of the proposed technique is a classification stage, in which different neural networks perform a classification of the image pixels to detect the IMT contours (LI and MA interfaces). Networks take as input information only the intensity values from a neighbourhood (13×3) of the pixel to be classified. The suggested architecture includes auto-encoders to obtain compressed and efficient representations of the input data. These auto-encoders establish the basis for the design of deep networks to identify LII-pixels and MAI-pixels. The system is completed with a pre-processing stage in which ROI (far wall of the CCA) is automatically selected and with a post-processing stage for the extraction of the final contours on which the IMT is assessed.

The proposed configuration has been tested using a set of 55 ultrasound CCA images. The automatic segmentation achieves the

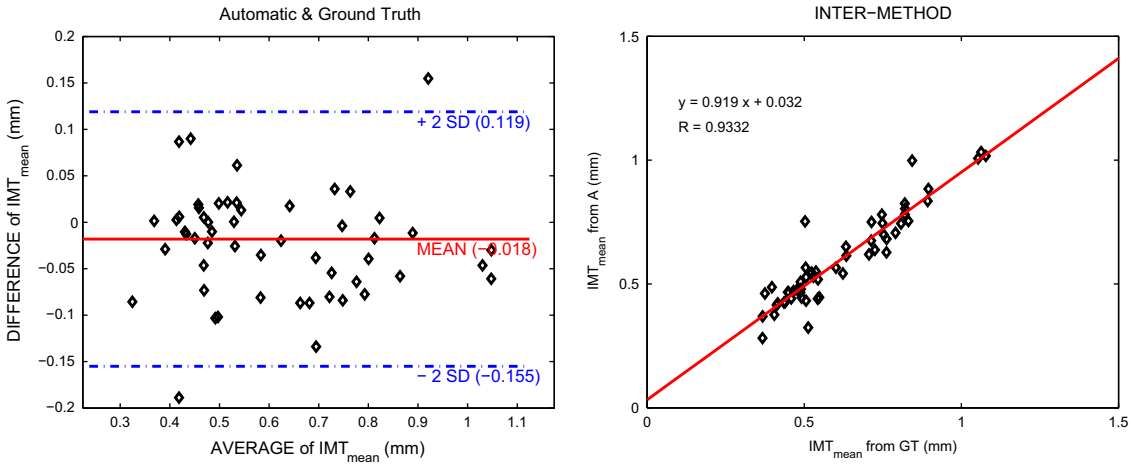

Fig. 9. Statistical distribution of the IMT measurement errors. BlandAltman plot (left) and linear regression analysis (right).

correct detection of the LI and MA interfaces in all the tested images. Furthermore, the automatic measurements of IMT have been compared with the values obtained from manual tracings and several quantitative statistical evaluations have shown the accuracy and robustness of the suggested approach.

The main advantage of the CCA segmentation method proposed in this paper is its computational efficiency, with a mean total time per processed image of 1.4 s. This fact together with the high agreement between automatic and manual segmentations makes this method a suitable solution for the clinical evaluation of IMT. Besides, with this average execution time, the method could also be used for the segmentation of ultrasound CCA videos. Future works must study the use of different learning machines (support vector machines, extreme learning machines) to construct the proposed deep networks. However, although the MLP solution used in this work seems to be the simplest, it provides quite satisfactory results.

References

[1] W.H. Organization, Global Atlas on Cardiovascular Disease Prevention and Control, Online, URL: ⟨www.who.int/cardiovascular_diseases/en/⟩.

[2] P.-J. Touboul, et al., Mannheim carotid intima-media thickness and plaque consensus (2004–2006–2011), Cerebrovasc. Dis. 34 (2012) 290–296.

[3] M. Bots, G.W. Evans, W. Riley, D. Grobbee, Carotid intima-media thickness measurements in intervention studies: design options, progression rates, and sample size considerations—a point of view, Stroke 34 (12) (2003) 2985–2994.

[4] J. Gonzalez, J. Wood, F.J. Dorey, T.A.L. Wren, V. Gilsanz, Reproducibility of carotid intima-media thickness measurements in young adults, Radiology 247 (2) (2008) 247–465.

[5] F. Molinari, G. Zeng, J.S. Suri, Review: a state of the art review on intima-media thickness (imt) measurement and wall segmentation techniques for carotid ultrasound, Comput. Methods Prog. Biomed. 100 (3) (2010) 201–221.

[6] C. Liguori, A. Paolillo, A. Pietrosanto, An automatic measurement system for the evaluation of carotid intima-media thickness, IEEE Trans. Instrum. Meas. 50 (6) (2001) 1684–1691.

[7] D.-C. Cheng, A. Schmidt-Trucksass, K.-S. Cheng, H. Burkhardt, Using snakes to detect the intimal and adventitial layers of the common carotid artery wall in sonographic images, Comput. Methods Prog. Biomed. 67 (1) (2002) 27–37.

[8] J.H. Stein, C.E. Korcarz, M.E. Mays, P.S. Douglas, M. Palta, H. Zhang, T. LeCaire, D. Paine, D. Gustafson, L. Fan, A semiautomated ultrasound border detection program that facilitates clinical measurement of ultrasound carotid intima-media thickness, J. Am. Soc. Echocardiogr. 18 (3) (2005) 244–251.

[9] F. Faita, V. Gemignani, E. Bianchini, C. Giannarelli, L. Ghiadoni, M. Demi, Real-time measurement system for evaluation of the carotid intima-media thickness with a robust edge operator, J. Ultrasound Med. 27 (9) (2008) 1353–1361.

[10] R. Rocha, A. Campilho, J. Silva, E. Azevedo, R. Santos, Segmentation of the carotid intima-media region in b-mode ultrasound images, Image Vis. Comput. 28 (4) (2010) 614–625.

[11] R.-M. Menchón-Lara, M.-C. Bastida-Jumilla, J. Morales-Sánchez, J.-L. Sancho-Gómez, Automatic detection of the intima-media thickness in ultrasound images of the common carotid artery using neural networks, Med. Biol. Eng. Comput. 52 (2) (2014) 169–181.

[12] S. Delsanto, F. Molinari, P. Giusetto, W. Liboni, S. Badalamenti, J. Suri, Characterization of a completely user-independent algorithm for carotid artery segmentation in 2-d ultrasound images, IEEE Trans. Instrum. Meas. 56 (4) (2007) 1265–1274.

[13] S. Golemati, J. Stoitsis, E.G. Sifakis, T. Balkizas, K.S. Nikita, Using of the hough transform to segment ultrasound images of longitudinal and transverse sections of the carotid artery, Ultrasound Med. Biol. 33 (12) (2007) 1918–1932.

[14] F. Molinari, G. Zeng, J. Suri, Intima-media thickness: setting a standard for a completely automated method of ultrasound measurement, IEEE Trans. Ultrason., Ferroelectr. Freq. Control 57 (5) (2010) 1112–1124.

[15] M.C. Bastida-Jumilla, R.M. Menchón-Lara, J. Morales-Sánchez, R. Verdú-Monedero, J. Larrey-Ruiz, J.L. Sancho-Gómez, Segmentation of the common carotid artery walls based on a frequency implementation of active contours, J. Digit. Imaging 26 (1) (2013) 129–139.

[16] R.H. Selzer, W.J. Mack, P.L. Lee, H. Kwong-Fu, H.N. Hodis, Improved common carotid elasticity and intima-media thickness measurements from computer analysis of sequential ultrasound frames, Atherosclerosis 154 (1) (2001) 185–193.

[17] I. Wendelhag, Q. Liang, T. Gustavsson, J. Wikstrand, A new automated computerized analysis system simplifies readings and reduces the variability in ultrasound measurement of intima-media thickness, Stroke 28 (1997) 2195–2200.

[18] Q. Liang, I. Wendelhag, J. Wikstrand, T. Gustavsson, A multiscale dynamic programming procedure for boundary detection in ultrasonic artery images, IEEE Trans. Med. Imaging 19 (2) (2000) 127–142.

[19] T. Gustavsson, Q. Liang, I. Wendelhag, J. Wikstrand, A dynamic programming procedure for automated ultrasonic measurement of the carotid artery, in: Computers in Cardiology, 1994, pp. 297–300.

[20] D.-C. Cheng, X. Jiang, Detections of arterial wall in sonographic artery images using dual dynamic programming, IEEE Trans. Inf. Technol. Biomed. 12 (6) (2008) 792–799.

[21] N. Santhiyakumari, M. Madheswaran, Non-invasive evaluation of carotid artery wall thickness using improved dynamic programming technique, Signal, Image Vid. Process. 2 (2) (2008) 183–193.

[22] Y.-B. Lee, Y.-J. Choi, M.-H. Kim, Boundary detection in carotid ultrasound images using dynamic programming and a directional haar-like filter, Comput. Biol. Med. 40 (8) (2010) 687–697.

[23] R. Chan, J. Kaufhold, L. Hemphill, R. Lees, W. Karl, Anisotropic edge-preserving smoothing in carotid b-mode ultrasound for improved segmentation and intima-media thickness (imt) measurement, in: Computers in Cardiology, 2000, pp. 37–40.

[24] M. Gutierrez, P. Pilon, S. Lage, L. Kopel, R. Carvalho, S. Furuie, Automatic measurement of carotid diameter and wall thickness in ultrasound images, in: Computers in Cardiology, 2002, pp. 359–362.

[25] C.P. Loizou, C.S. Pattichis, M. Pantziaris, T. Tyllis, A. Nicolaides, Snakes based segmentation of the common carotid artery intima media, Med. Biol. Eng. Comput. 45 (1) (2007) 35–49.

[26] M. Ceccarelli, N. De Luca, A. Morganella, An active contour approach to automatic detection of the intima-media thickness, in: 2006 IEEE International Conference on Acoustics, Speech and Signal Processing (ICASSP), vol. 5, 2006, pp. 709–712.

[27] F. Molinari, K.M. Meiburger, L. Saba, U.R. Acharya, M. Ledda, A. Nicolaides, J.S. Suri, Constrained snake vs. conventional snake for carotid ultrasound automated imt measurements on multi-center data sets, Ultrasonics 52 (7) (2012) 949–961.

[28] S. Petroudi, C. Loizou, M. Pantziaris, C. Pattichis, Segmentation of the common carotid intima-media complex in ultrasound images using active contours, IEEE Trans. Biomed. Eng. 59 (11) (2012) 3060–3069.
[29] G. Liu, B. Wang, D. Liu, Detection of intima-media layer of common carotid artery with dynamic programming based active contour model, in: Chinese Conference on Pattern Recognition (CCPR'08), 2008, pp. 1–6.
[30] F. Destrempes, J. Meunier, M.-F. Giroux, G. Soulez, G. Cloutier, Segmentation in ultrasonic b-mode images of healthy carotid arteries using mixtures of Nakagami distributions and stochastic optimization, IEEE Trans. Med. Imaging 28 (2) (2009) 215–229.
[31] D. Ilea, P. Whelan, C. Brown, A. Stanton, An automatic 2d cad algorithm for the segmentation of the imt in ultrasound carotid artery images, in: Annual International Conference of the IEEE Engineering in Medicine and Biology Society (EMBC 2009), 2009, pp. 515–519.
[32] X. Xu, Y. Zhou, X. Cheng, E. Song, G. Li, Ultrasound intima-media segmentation using hough transform and dual snake model, Comput. Med. Imaging Graph. 36 (3) (2012) 248–258.
[33] R.C. González, R.E. Woods, S.L. Eddins, Digital Image Processing Using Matlab, Pentice Hall, Englewood Cliffs, NJ, 2004.
[34] D. Pham, C. Xu, J. Prince, Current methods in medical image segmentation, Ann. Rev. Biomed. Eng. 2 (2000) 315–337.
[35] M. Moller, A scaled conjugate gradient algorithm for fast supervised learning, Neural Netw. 6 (1993) 525–533.
[36] G.E. Hinton, R.R. Salakhutdinov, Reducing the dimensionality of data with neural networks, Science 313 (5786) (2006) 504–507.
[37] L.L.C. Kasun, H. Zhou, G.-B. Huang, C.M. Vong, Representational learning with extreme learning machine for big data, IEEE Intell. Syst. 28 (6) (2013) 31–34.

Rosa-María Menchón-Lara was born in 1985 in Murcia, Spain. She received the M.S. degree in Telecommunication Engineering in 2009 from Universidad Politécnica de Cartagena (Spain). She is currently pursuing her Ph. D. degree at the same university. Her research interests are Machine Learning, Artificial Neural Networks, Digital Signal Processing, Statistical Pattern Recognition, and Image Processing.

José Luis Sancho-Gómez received his Physics degree from the Universidad de La Laguna, Tenerife (Spain) in 1992, his M.S in Electrical Engineering from the Universidad Politécnica de Madrid, Madrid (Spain) in 1994, and his Ph.D. in Electrical Engineering from the Universidad Carlos III de Madrid, Madrid (Spain) in 1999. Currently, he is an Associate Professor at the Universidad Politécnica de Cartagena, Murcia (Spain). His research interests include Digital Signal Processing, Statistical Pattern Recognition, Neural Networks, and Machine Learning.